JOURNAL OF BACTERIOLOGY, Dec. 2007, p. 8801–8806 Vol. 189, No. 24
0021-9193/07/$08.00+0 doi:10.1128/JB.01299-07

Single-Molecule Force Spectroscopy of Mycobacterial Adhesin-Adhesin Interactions[▽]

Claire Verbelen,[1] Dominique Raze,[2,3,4] Frédérique Dewitte,[3,4,5] Camille Locht,[2,3,4] and Yves F. Dufrêne[1]*

Unité de Chimie des Interfaces, Université Catholique de Louvain, Croix du Sud 2/18, B-1348 Louvain-la-Neuve, Belgium[1]; INSERM, U629, Mécanismes Moléculaires de la Pathogénie Microbienne, Lille, France[2]; Institut Pasteur de Lille, 1 rue du Professeur Calmette, F-59019 Lille Cedex, France[3]; IFR 142, Molecular and Cellular Medicine, Lille, France[4]; and CNRS UMR 8161, IBL, Lille, France[5]

Received 10 August 2007/Accepted 28 September 2007

The heparin-binding hemagglutinin (HBHA) is one of the few virulence factors identified for *Mycobacterium tuberculosis*. It is a surface-associated adhesin that expresses a number of different activities, including mycobacterial adhesion to nonphagocytic cells and microbial aggregation. Previous evidence indicated that HBHA is likely to form homodimers or homopolymers via a predicted coiled-coil region located within the N-terminal portion of the molecule. Here, we used single-molecule atomic-force microscopy to measure individual homophilic HBHA-HBHA interaction forces. Force curves recorded between tips and supports derivatized with HBHA proteins exposing their N-terminal domains showed a bimodal distribution of binding forces reflecting the formation of dimers or multimers. Moreover, the binding peaks showed elongation forces that were consistent with the unfolding of α-helical coiled-coil structures. By contrast, force curves obtained for proteins exposing their lysine-rich C-terminal domains showed a broader distribution of binding events, suggesting that they originate primarily from intermolecular electrostatic bridges between cationic and anionic residues rather than from specific coiled-coil interactions. Notably, similar homophilic HBHA-HBHA interactions were demonstrated on live mycobacteria producing HBHA, while they were not observed on an HBHA-deficient mutant. Together with the fact that HBHA mediates bacterial aggregation, these observations suggest that the single homophilic HBHA interactions measured here reflect the formation of multimers that may promote mycobacterial aggregation.

Mycobacterium tuberculosis, one of the most devastating microbial pathogens for humans, infects roughly one-third of the population worldwide and causes between 1.5 and 2 million deaths annually (15). Very few *M. tuberculosis* virulence factors have been identified so far. One of them is the 21-kDa heparin-binding hemagglutinin (HBHA), a 198-residue protein that recognizes heparan sulfate proteoglycans (16, 17, 23) on the surfaces of target cells (for a recent review, see reference 12).

HBHA acts as a multifunctional adhesin. It promotes bacterial aggregation (16), and in cell culture, it binds to epithelial cells, endothelial cells, and fibroblasts, but apparently not to macrophages. Binding to these target cells involves the C-terminal, lysine-rich domain of the protein, which contains the entire heparin-binding domain (22). This domain is exposed at the mycobacterial cell surface, as evidenced by immunogold electron microscopy using anti-HBHA monoclonal antibodies (16) and by atomic-force microscopy (AFM) (5). The N-terminal moiety of HBHA appears to be buried within the mycobacterial cell wall or involved in the formation of multimeric structures, as antibodies to this region do not decorate intact mycobacteria. It contains a predicted coiled-coil region, which is involved in homophilic interactions of HBHA (3). These homophilic interactions may potentially contribute to HBHA-mediated bacterial aggregation and/or to the formation of polymeric HBHA structures. However, detailed information on the nature and forces of such homophilic interactions is lacking.

Previously, we measured the specific interaction forces between HBHA and its model receptor heparin using AFM (5), a powerful technique that is being increasingly used to investigate the forces within or between single biomolecules (2, 7, 11, 19, 21, 25). This technique has allowed us to map single adhesin molecules on the surfaces of live mycobacteria, revealing that they were localized in discrete regions of the cell surface. Here, we used single-molecule AFM to investigate the molecular forces driving HBHA-HBHA interactions, both on model surfaces and on live mycobacteria.

MATERIALS AND METHODS

Bacterial strains and growth conditions. *Mycobacterium bovis* bacillus Calmette Guérin (BCG) 1173P and BCGΔHBHA, deficient for HBHA production (23), were grown in Sauton medium at 37°C for about 10 days (optical density at 600 nm, ~0.6) under static conditions using 75-cm^2 Roux flasks containing 50 ml of Sauton medium. The bacteria were harvested by centrifugation, washed three times with deionized water, and resuspended to a concentration of ~10^8 cells per ml. *Escherichia coli* BL21(DE3) containing the pET derivatives with the genes corresponding to the different HBHA variants was grown at 37°C under constant shaking in LB medium.

Preparation of recombinant HBHA derivatives. *E. coli* BL21(DE3)(pGD51) producing recombinant HBHA His tagged at the N terminus (rHBHA N-His) was described elsewhere (3) and was kindly provided by G. Delogu. To obtain recombinant HBHA His tagged at its C terminus (rHBHA C-His), pET-HBHAC was constructed as follows. The *hbhA* gene from genomic BCG DNA was amplified as a 371-bp fragment using the following primers: TCCGCTCG

* Corresponding author. Mailing address: Unité de Chimie des Interfaces, Université Catholique de Louvain, Croix du Sud 2/18, B-1348 Louvain-la-Neuve, Belgium. Phone: (32) 10 47 36 00. Fax: (32) 10 47 20 05. E-mail: dufrene@cifa.ucl.ac.be.

▽ Published ahead of print on 12 October 2007.

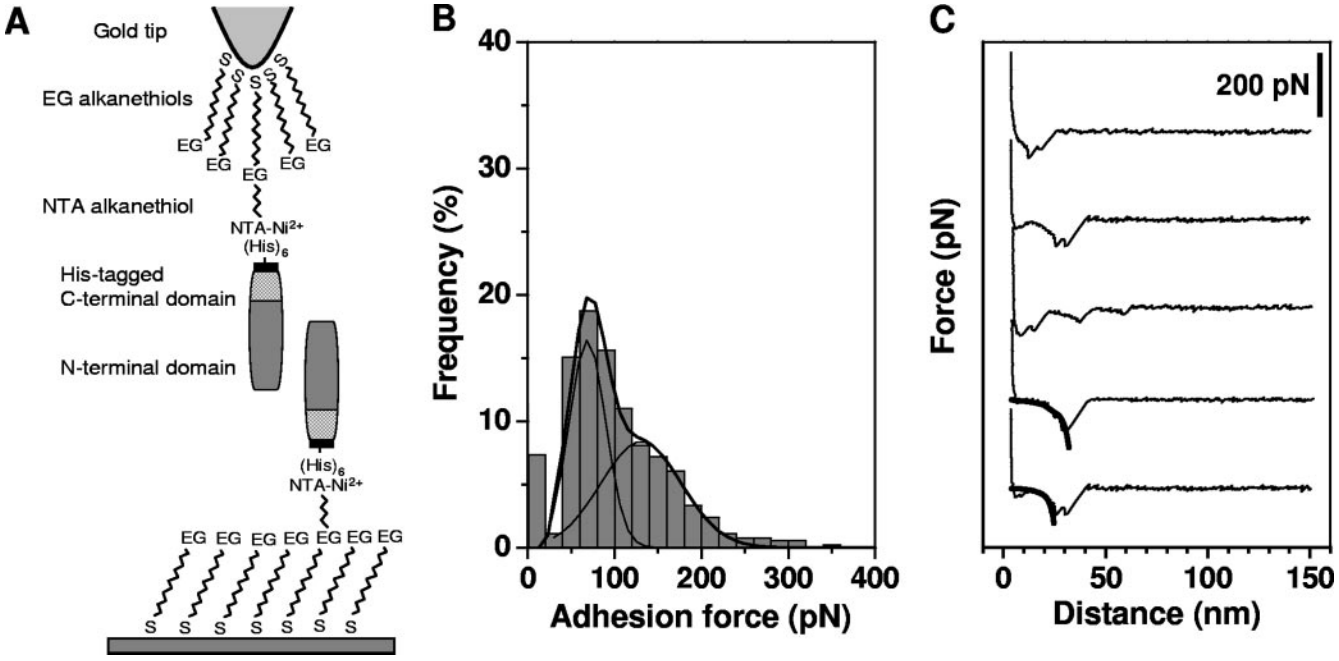

FIG. 1. Force spectroscopy of HBHA N-terminal domains. (A) Schematic of the surface chemistry used to functionalize AFM tips and supports with HBHAs having their N-terminal ends exposed. (B and C) Adhesion force histogram (B) (n = 512) and representative force curves (C) measured between N-terminal domains. All curves were obtained using a retraction speed of 1,000 nm s^{-1} and an interaction time of 500 ms. Elongation forces were generally well described by the worm-like-chain model (thick lines on bottom curves), using a persistence length of 0.4 nm, which is typical for proteins $\{F(x) = k_bT/l_p\,[0.25(1 - x/L_c)^{-2} + x/L_c - 0.25]$, where L_c and l_p are the contour length and persistence length of the molecule, k_b is the Boltzmann constant, and T is the absolute temperature$\}$.

AGGCCGCGACTAGCCGG and ACCCAAGCTTTCAGTGGTGGTGGTGG TGGTGCTTCTGGGTGACCTTCTT, corresponding at the 3′ end of *hbhA* to a sequence encoding six histidine residues. The amplicon was inserted into pCRIITopo (Invitrogen). A 406-bp XhoI fragment from this construct was then excised and used to replace the 495-bp XhoI fragment of pET-HBHA (22). The rHBHA N-His and rHBHA C-His molecules were purified by heparin-Sepharose chromatography as described elsewhere (17).

Aggregation bioassays. Aggregation assays were performed according to the procedure described previously (16). Polypropylene round-bottom tubes (Falcon; 17 by 100-mm style) were filled with 5 ml suspensions containing *M. bovis* BCG or the mutant *M. bovis* BCGΔHBHA deficient in HBHA production (23) in Sauton medium at a concentration of 10^8 bacterial cells per ml to which HBHA was added at various concentrations (0, 0.2, 0.5, 2, or 5 μg/ml). The tubes were agitated upside down at 25 rpm for 15 min, and 500 μl of each suspension was left undisturbed for 30 min before optical microscopy examination. Samples were observed with a Leica DMRA2 microscope using a PL Fluotar objective (40×/0.65 PH2).

Preparation and validation of HBHA-modified surfaces. Recombinant HBHA proteins bearing a His tag at their N-terminal or C-terminal end were immobilized onto gold-coated supports and AFM tips, using the specific binding between histidine tags and nitrilotriacetic acid (NTA)-terminated self-assembled monolayers. AFM cantilevers (Microlevers; Veeco Metrology Group, Santa Barbara, CA) and silicon wafers (Siltronix, France) were coated using electron beam thermal evaporation with a 5-nm-thick Cr layer followed by a 30-nm thick Au layer. Before use, the gold-coated cantilevers and supports were cleaned for 5 min by UV/ozone treatment (Jelight Co., Irvine, CA), rinsed with ethanol, and dried with a gentle nitrogen flow. They were immersed overnight in ethanol solutions containing 0.05 mM of NTA-terminated (20%) and tri(ethylene glycol) (EG)-terminated (80%) alkanethiols (kindly supplied by N. L. Abbott) (see reference 13 for details on the synthesis of these molecules) and rinsed with ethanol. Sonication was briefly applied to remove alkanethiol aggregates that may have been adsorbed. Then, surfaces were immersed in 40 mM $NiSO_4$ (pH 7.2) for 1 h and rinsed with phosphate-buffered saline (PBS). Finally, the samples were incubated in PBS containing 2 μg/ml His-tagged peptides for 2 h and further rinsed several times with PBS.

The quality of the above-mentioned surface modifications was assessed using X-ray photoelectron spectroscopy (XPS). Supports were rinsed with water and dried by flushing them with a gentle nitrogen flow and then immediately introduced into the XPS vacuum chamber. The analyses were performed on a Kratos Axis Ultra spectrometer (Kratos Analytical, United Kingdom) equipped with a monochromatized aluminum X-ray source. The samples were fixed on a stainless-steel multispecimen holder by using double-sided conductive tape. The angle between the normal to the sample surface and the electrostatic lens axis was 0°. The analyzed area was ~700 μm by 300 μm. The constant pass energy of the hemispherical analyzer was set at 40 eV. The following sequence of spectra was recorded: survey spectrum, C_{1s}, N_{1s}, O_{1s}, Au_{4f}, S_{2p}, and C_{1s} again to check the stability of charge compensation as a function of time and the absence of degradation of the sample during the analyses. The binding energies were calculated with respect to the *C*-(C,H) component of the C1s peak of adventitious carbon fixed at 284.8 eV. Following subtraction of a linear baseline, molar fractions were calculated (CasaXPS program; Casa Software Ltd., United Kingdom) using peak areas normalized on the basis of acquisition parameters, sensitivity factors, and the transmission function provided by the manufacturer.

AFM measurements. AFM images and force-distance curves were obtained in PBS at room temperature, using a Nanoscope IV Multimode AFM (Veeco Metrology Group, Santa Barbara, CA). The bottom side of hydrated supports was quickly dried using precision wipes (Kimwipes; Kimberly-Clark), and the supports were then immobilized on a steel sample puck using a small piece of adhesive tape. The mounted samples were immediately transferred into the AFM liquid cell, while avoiding dewetting. Force measurements were performed with triangular-shaped silicon nitride cantilevers functionalized as described above. All curves were recorded with a maximum applied force of ~400 pN. To estimate the spring constants of the cantilevers, we measured their geometrical dimensions using scanning electron microscopy, as well as their free resonance frequencies. Then, the cantilever's mechanical properties were adjusted in order to match the calculated frequencies to the measured ones. The determined mechanical properties and the measured geometrical dimensions were then used to calculate the spring constants, which were typically ~0.01 N/m.

To image mycobacteria in their native state by AFM, the cells were immobilized by mechanical trapping onto porous polycarbonate membranes (Millipore), with a pore size similar to the bacterial cell size. This approach is well suited to image single cells under aqueous conditions, and it does not involve chemical

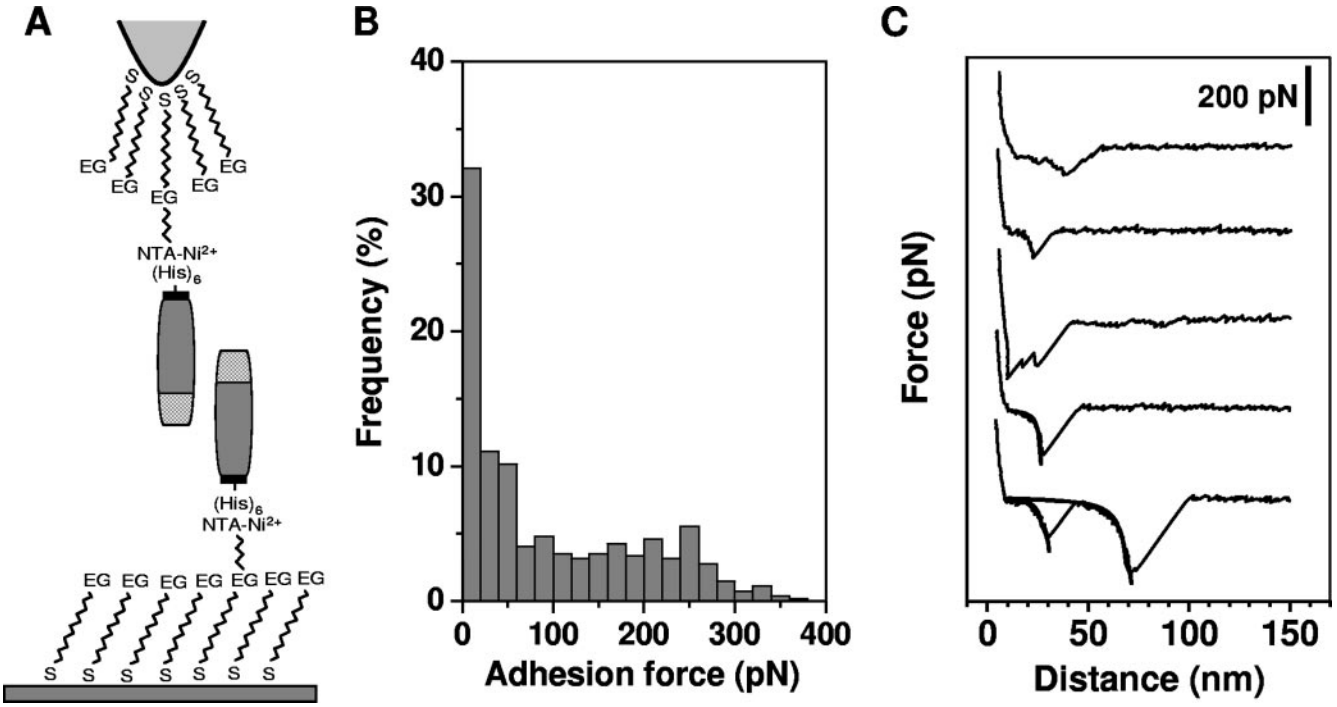

FIG. 2. Force spectroscopy of HBHA C-terminal domains. (A) Schematic of the surface chemistry used to functionalize AFM tips and supports with HBHAs having their C-terminal ends exposed. (B and C) Adhesion force histogram (B)(n = 512) and representative force curves (C) measured between C-terminal domains. All curves were obtained using a retraction speed of 1,000 nm s^{-1} and an interaction time of 500 ms. Elongation forces were generally well described by the worm-like-chain model (thick lines on bottom curves), using a persistence length of 0.4 nm.

treatment or drying, which would cause rearrangement or denaturation of the surface molecules (4). After a concentrated cell suspension was filtered, the filter was gently rinsed with deionized water, carefully cut (1 cm by 1 cm), and attached to a steel sample puck (Veeco Metrology Group) using a small piece of adhesive tape, and the mounted sample was transferred into the AFM liquid cell.

RESULTS AND DISCUSSION

Forces and dynamics of HBHA-HBHA interactions. The 157-residue-long N-terminal domain of HBHA contains a large predicted coiled-coil region that extends over 81 amino acids (3). This predicted coiled-coil region is composed of heptad repeats with a number of predicted α-helical turns, suggesting that the protein has an extended rather than a globular conformation. The ability of the coiled-coil region to form multimers has been previously reported (3). However, the interaction forces driving multimer formation remain essentially unknown.

To address HBHA-HBHA interactions at the level of single molecules, genetically engineered histidine-tagged proteins were attached, via their C-terminal or N-terminal ends, to gold-coated AFM tips and supports modified with Ni^{2+}-NTA and tri-EG-terminated alkanethiols, a method that allows proteins to be uniformly oriented at low density (Fig. 1A and 2A). The quality of the adhesin-functionalized surfaces was checked by XPS. Table 1 presents the surface chemical compositions determined by XPS for gold supports after the main steps of the immobilization procedure. Gold surfaces treated with NTA/EG-terminated alkanethiols showed significant oxygen, sulfur, and nitrogen concentrations, indicating the presence of an NTA/EG-terminated monolayer. Incubation with Ni^{2+} and HBHA His tagged at the C-terminal or N-terminal end led to an increase of the nitrogen concentration, reflecting the presence of substantial amounts of adhesins at the surface.

Force-distance curves were first recorded between HBHAs exposing their N-terminal regions, using a pulling speed of 1,000 nm/s and an interaction time of 500 ms (Fig. 1B and C). Most retraction curves displayed single binding peaks together with nonlinear elongation forces, yielding a binding force histogram with two maxima centered at 68 ± 2 pN and 130 ± 14 pN (n = 512). For two reasons, this bimodal distribution likely reflects the formation of one and two HBHA dimers, respectively, resulting from specific coiled-coil interactions: (i) coiled-coil domains are known to promote the formation of oligomeric structures (14); (ii) HBHA is known to form dimers and multimers (3). In fact, it is tempting to attribute the two binding peaks to lateral oligomerization and cooperative unbinding of HBHA dimers, rather than to the disruption of two independent dimers as previously proposed for cadherins (1).

TABLE 1. Surface chemical compositions of solid supports functionalized with HBHA exposing their N-terminal and C-terminal ends

Sample	Mole fraction (%)[a]				
	Au	C	S	O	N
NTA/EG	57.0	32.7	2.7	5.6	2.0
NTA/EG + $HBHA_{Nterm}$	38.3	43.5	1.9	9.7	6.6
NTA/EG + $HBHA_{Cterm}$	29.7	48.5	2.0	11.3	8.5

[a] Mole fraction of elements excluding hydrogen.

Most binding events showed nonlinear elongation forces (Fig. 1C) that were best described by the worm-like-chain model, classically used to model the unfolding of polypeptide chains (20, 26). Because HBHA monomers can be picked up anywhere along their tails, large variations in contour lengths were observed (from 16 to 32 nm). Nevertheless, they were always smaller than the 72-nm length expected for a fully stretched, 198-residue HBHA polypeptide chain (assuming an unfolded length of 3.6 Å per amino acid). The stretching distance, i.e., the distance over which elongation occurred, varied from 8 to 19 nm, which is in the range of the length difference expected between a folded and an unfolded HBHA coiled coil. Assuming the folded and unfolded lengths of an amino acid are 1.4 Å and 3.6 Å, respectively, the increase in length expected for an 81-amino-acid polypeptide would be 18 nm (28). The notion that α-helices are being unfolded is further supported by the observation of fairly small (68 ± 2 pN) binding forces (9, 10, 27). By way of comparison, much larger forces (150 to 300 pN) are required to unfold domains with β-folds, like immunoglobulin or fibronectin domains in titin and tenascin (20, 26). The above observations lead us to believe that the measured elongation forces reflect the unfolding of α-helices of the coiled-coil domain.

When the forces between HBHA proteins exposing their lysine-rich C-terminal domains were measured, the binding events showed a much broader distribution (Fig. 2). The lack of a well-defined maximum, together with the larger average binding force values (137 ± 91 pN), suggests that these forces do not primarily originate from specific coiled-coil interactions. The main contribution is probably due to multiple intermolecular electrostatic bridges between the cationic groups of the C-terminal, lysine-rich region and anionic aspartates/glutamates of the protein, as similar ionic bridges mediate the interaction of the C-terminal domain with heparin (5, 22) and heparan sulfate proteoglycans on the surfaces of epithelial cells (3, 22). In addition, most elongation forces were well fitted by the worm-like-chain model, suggesting that α-helices of the coiled-coil domain were also unfolded. In summary, different binding forces were measured for the N-terminal and C-terminal HBHA tails and attributed to specific interactions reflecting the association of α-helices into coiled-coil structures and to electrostatic interactions between cationic and anionic residues, respectively.

The forces necessary to rupture specific bonds are known to depend on the pulling speed (1, 5, 6, 18). Consistent with these studies, we found that the binding force between the N-terminal domains increased linearly with the logarithm of the pulling speed (Fig. 3A). Strikingly, we found the same dependence for the C-terminal domains, suggesting that intermolecular electrostatic bridges are stronger when they are pulled faster. We also studied the variation of binding frequency (i.e., the number of curves with adhesion events) with interaction time, while keeping the pulling speed constant (Fig. 3B). The binding frequency of the N-terminal region reached a plateau corresponding to almost 100% binding probability after only 0.1 s, indicating that bond formation is fast. This process is reminiscent of the VE-cadherin situation, where the probability of forming dimers was shown to be maximal after only 0.2 s (1). By contrast, the binding frequency of the C-terminal region increased only slowly with contact time to reach 60% binding probability after 1 s. This fairly slow binding process, resembling that observed for the HBHA-heparin interaction (5), is consistent with the idea that a prolonged interaction time is necessary to allow optimal fitting between positive and negative charges within HBHA monomers.

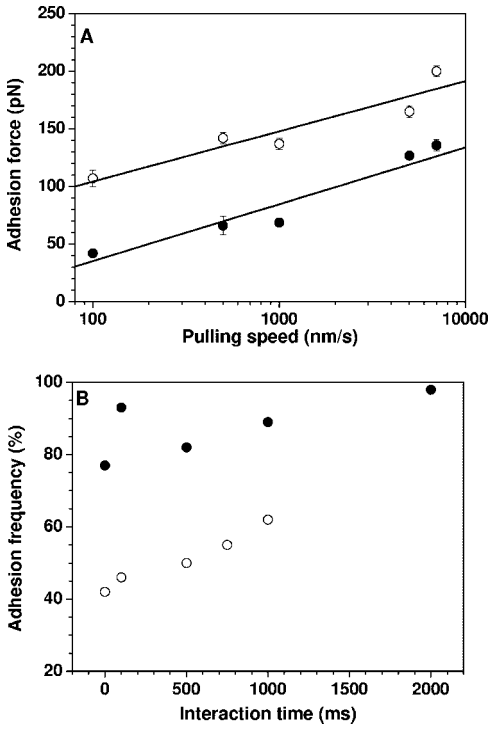

FIG. 3. Dynamics of HBHA-HBHA interactions. (A) Plot of the adhesion force measured between HBHAs having either their N-terminal (closed symbols) or C-terminal (open symbols) ends exposed as a function of the logarithm of the pulling speed applied during retraction while keeping constant the interaction time (500 ms) and the approach speed (1,000 nm/s). The data represent the means of 512 measurements (the standard errors of the mean are visible on the graph). (B) Plot of the adhesion frequency as a function of the interaction time, measured at a constant approach and retraction speed of 1,000 nm/s. The data represent the means of 512 measurements.

Homophilic HBHA-HBHA interactions are involved in mycobacterial aggregation. It has been shown that HBHA can induce mycobacterial aggregation (16). To assess whether this aggregation may result from homotypic HBHA-HBHA interactions, we compared HBHA-induced aggregation of *M. bovis* BCG with that of an HBHA-deficient BCG mutant (23). Optical microscopy was used to observe the different BCG cells after incubation with recombinant HBHA used at various concentrations (Fig. 4). The addition of HBHA to BCG suspensions promoted mycobacterial aggregation in a dose-dependent manner (Fig. 4A), as previously described (16). By contrast, the mutant strain lacking HBHA did not significantly aggregate by the addition of HBHA (Fig. 4B). These observations indicate that the production of endogenous HBHA is required for HBHA-mediated mycobacterial aggregation and are thus consistent with the contention that mycobacterial aggregation involves homophilic HBHA-HBHA interactions.

Homophilic HBHA-HBHA binding forces on live bacteria. To determine whether the measured binding forces using re-

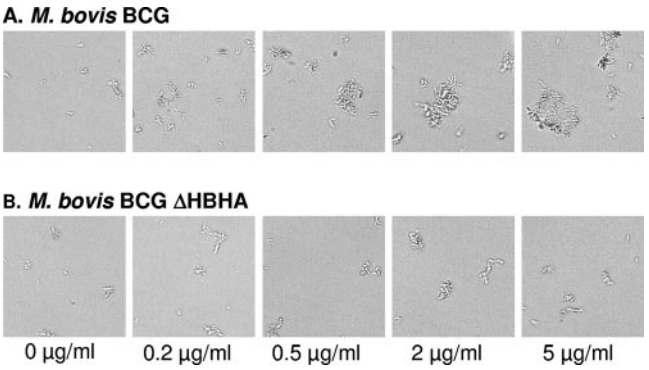

FIG. 4. Aggregation of mycobacteria upon incubation with HBHA. Optical micrographs (image size, 60 μm) of *M. bovis* BCG (A) and of a mutant strain lacking HBHA (B) after incubation with HBHA at 0, 0.2, 0.5, 2, or 5 μg protein/ml. Upon injection of 5 μg protein/ml, the average size of bacterial aggregates increased from 80 ± 51 μm^2 to 382 ± 310 μm^2 for *M. bovis* BCG, while it only increased from 51 ± 22 μm^2 to 70 ± 54 μm^2 for the mutant.

combinant HBHA molecules are similar to the homophilic HBHA-HBHA interaction forces on mycobacteria, HBHA tips were used to probe the surfaces of live BCG cells (Fig. 5). High-resolution topographic images revealed a smooth and homogeneous surface, consistent with an earlier report (5). Force-distance curves recorded over 400-nm by 400-nm areas with a tip exposing N-terminal regions exhibited a distribution reminiscent of that observed for model surfaces exposing N-terminal tails (Fig. 1) and attributed to multimer formation due to specific coiled-coil interactions. Although defining a bimodal distribution was rather delicate and questionable, such decomposition yielded average forces of 99 ± 3 pN and 212 ± 7 pN, larger than the forces on model surfaces. This difference may be due to differences in the binding mechanism

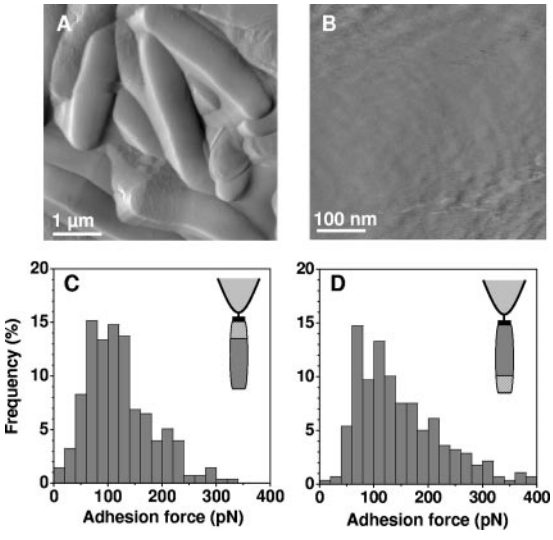

FIG. 5. Probing HBHA-HBHA interactions on *M. bovis* BCG. Low-resolution (A) and high-resolution (B) AFM images of *M. bovis* BCG cells. (C and D) Adhesion force histograms (n = 256) obtained with an AFM tip exposing N-terminal (C) or C-terminal (D) ends, using a constant pulling speed (1,000 nm/s during both approach and retraction) and interaction time (500 ms).

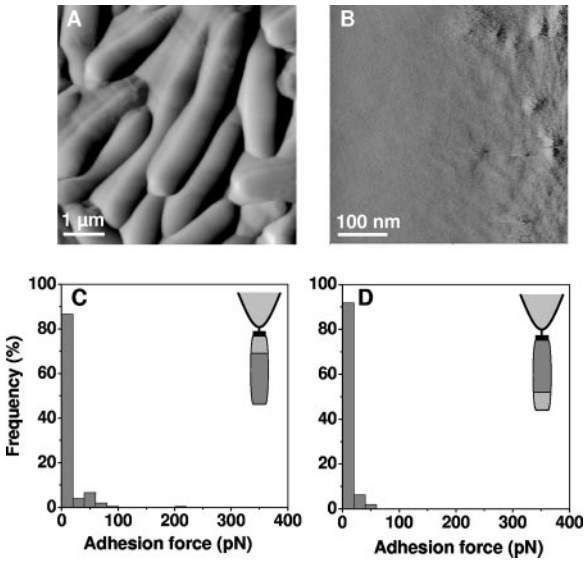

FIG. 6. Probing HBHA-HBHA interactions on an *M. bovis* BCG mutant lacking HBHA. Low-resolution (A) and high-resolution (B) AFM images of mutant cells are shown. (C and D) Adhesion force histograms (n = 256) obtained with an AFM tip exposing N-terminal (C) or C-terminal (D) ends, using a constant pulling speed (1,000 nm/s during both approach and retraction) and interaction time (500 ms).

(e.g., multimers with different natures) or to posttranslational modifications of HBHA occurring on the bacterial surface, as native HBHA has been shown to be methylated (24).

The tips exposing C-terminal regions also showed binding forces in most areas, but a broader distribution was observed, somewhat similar to that observed for model surfaces exposing C-terminal tails. Hence, it is possible that these forces originate from electrostatic interactions rather than from specific coiled-coil interactions. As a control, similar measurements were performed on the mutant lacking HBHA (Fig. 6). As expected, significant binding forces were not observed, using tips exposing either N-terminal or C-terminal tails, confirming that the forces measured on *M. bovis* BCG are due to HBHA-HBHA interactions.

Taken together, these data support the notions that (i) specific HBHA-HBHA interactions occur at the bacterial surface and (ii) these interactions are likely due to coiled-coil interactions via the N-terminal domains of HBHA. In light of the aggregation assays, we conclude that these interactions are likely to represent the main driving force for bacterial aggregation. This study offers new prospects for understanding the molecular basis of adhesion and aggregation processes and for testing novel antiadhesin drugs.

ACKNOWLEDGMENTS

We dedicate this article to the memory of Franco D. Menozzi.

This work was supported by the National Foundation for Scientific Research (FNRS), the Foundation for Training in Industrial and Agricultural Research (FRIA), the Université Catholique de Louvain (Fonds Spéciaux de Recherche), and the Federal Office for Scientific, Technical and Cultural Affairs (Interuniversity Poles of Attraction Programme). Y.F.D. is a Research Associate of the FNRS.

We thank V. Dupres for valuable discussions.

REFERENCES

1. **Baumgartner, W., P. Hinterdorfer, W. Ness, A. Raab, D. Vestweber, H. Schindler, and D. Drenckhahn.** 2000. Cadherin interaction probed by atomic force microscopy. Proc. Natl. Acad. Sci. USA **97:**4005–4010.
2. **Benoit, M., D. Gabriel, G. Gerisch, and H. E. Gaub.** 2000. Discrete interactions in cell adhesion measured by single-molecule force spectroscopy. Nat. Cell Biol. **2:**313–317.
3. **Delogu, G., and M. J. Brennan.** 1999. Functional domains present in the mycobacterial hemagglutinin, HBHA. J. Bacteriol. **181:**7464–7469.
4. **Dufrêne, Y. F.** 2004. Using nanotechniques to explore microbial surfaces. Nat. Rev. Microbiol. **2:**451–460.
5. **Dupres, V., F. D. Menozzi, C. Locht, B. H. Clare, N. L. Abbott, S. Cuenot, C. Bompard, D. Raze, and Y. F. Dufrêne.** 2005. Nanoscale mapping and functional analysis of individual adhesins on living bacteria. Nat. Methods **2:**515–520.
6. **Evans, E., and K. Richie.** 1997. Dynamic strength of molecular adhesion bonds. Biophys. J. **72:**1541–1555.
7. **Hinterdorfer, P., W. Baumgartner, H. J. Gruber, K. Schilcher, and H. Schindler.** 1996. Detection and localization of individual antibody-antigen recognition events by atomic force microscopy. Proc. Natl. Acad. Sci. USA **93:**3477–3481.
8. **Hodak, H., B. Clantin, E. Willery, V. Villeret, C. Locht, and F. Jacob-Dubuisson.** 2006. Secretion signal of the filamentous haemagglutinin, a model two-partner secretion substrate. Mol. Microbiol. **61:**368–382.
9. **Janovjak, H., J. Struckmeier, M. Hubain, A. Kedrov, M. Kessler, and D. J. Müller.** 2004. Probing the energy landscape of the membrane protein bacteriorhodopsin. Structure **12:**871–879.
10. **Lee, G., K. Abdi, Y. Jiang, P. Michaely, V. Bennett, and P. E. Marszalek.** 2006. Nanospring behaviour of ankyrin repeats. Nature **440:**246–249.
11. **Lee, G. U., L. A. Chrisey, and R. J. Colton.** 1994. Direct measurement of the forces between complementary strands of DNA. Science **266:**771–773.
12. **Locht, C., D. Raze, C. Rouanet, C. Genisset, J. Segers, and F. Mascart.** The mycobacterial heparin-binding hemagglutinin, virulence factor and antigen useful for diagnostics and vaccine development. *In* M. Daffé, and J.-M. Reyrat (ed.), The mycobacterial cell wall, in press. ASM Press, Washington, DC.
13. **Luk, Y.-Y., M. L. Tingey, D. J. Hall, B. A. Israel, C. J. Murphy, P. J. Bertics, and N. L. Abbott.** 2003. Using liquid crystals to amplify protein-receptor interactions: design of surfaces with nanometer-scale topography that present histidine-tagged protein receptors. Langmuir **19:**1671–1680.
14. **Lupas, A.** 1996. Coiled coils: new structures and new functions. Trends Biochem. Sci. **21:**375–382.
15. **Mandavilli, A.** 2007. A clash of cultures. Nat. Med. **13:**268–270.
16. **Menozzi, F. D., J. H. Rouse, M. Alavi, M. Laude-Sharp, J. Muller, R. Bischoff, M. J. Brennan, and C. Locht.** 1996. Identification of a heparin-binding hemagglutinin present in mycobacteria. J. Exp. Med. **184:**993–1001.
17. **Menozzi, F. D., R. Bischoff, E. Fort, M. J. Brennan, and C. Locht.** 1998. Molecular characterization of the mycobacterial heparin-binding hemagglutinin, a mycobacterial adhesin. Proc. Natl. Acad. Sci. USA **95:**12625–12630.
18. **Merkel, R., P. Nassoy, A. Leung, K. Ritchie, and E. Evans.** 1999. Energy landscapes of receptor-ligand bonds explored with dynamic force spectroscopy. Nature **397:**50–53.
19. **Nevo, R., C. Stroh, F. Kienberger, D. Kaftan, V. Brumfeld, M. Elbaum, Z. Reich, and P. Hinterdorfer.** 2003. A molecular switch between alternative conformational states in the complex of Ran and importin β1. Nat. Struct. Biol. **10:**553–557.
20. **Oberhauser, A. F., P. E. Marszalek, H. P. Erickson, and J. M. Fernandez.** 1998. The molecular elasticity of the extracellular matrix protein tenascin. Nature **393:**181–185.
21. **Oesterhelt, F., D. Oesterhelt, M. Pfeiffer, A. Engel, H. E. Gaub, and D. J. Müller.** 2000. Unfolding pathways of individual bacteriorhodopsins. Science **288:**143–146.
22. **Pethe, K., M. Aumercier, E. Fort, C. Gatot, C. Locht, and F. D. Menozzi.** 2000. Characterization of the heparin-binding site of the mycobacterial heparin-binding hemagglutinin adhesin. J. Biol. Chem. **275:**14273–14280.
23. **Pethe, K., S. Alonso, F. Biet, G. Delogu, M. J. Brennan, C. Locht, and F. D. Menozzi.** 2001. The heparin-binding haemagglutinin of *M. tuberculosis* is required for extrapulmonary dissemination. Nature **412:**190–194.
24. **Pethe, K., P. Bifani, H. Drobecq, C. Sergheraert, A.-S. Debrie, C. Locht, and F. D. Menozzi.** 2002. Mycobacterial heparin-binding hemagglutinin and laminin-binding protein share antigenic methyllysines that confer resistance to proteolysis. Proc. Natl. Acad. Sci. USA **99:**10759–10764.
25. **Rief, M., F. Oesterhelt, B. Heymann, and H. E. Gaub.** 1997. Single molecule force spectroscopy on polysaccharides by atomic force microscopy. Science **275:**1295–1297.
26. **Rief, M., M. Gautel, F. Oesterhelt, J. M. Fernandez, and H. E. Gaub.** 1997. Reversible unfolding of individual titin immunoglobulin domains by AFM. Science **276:**1109–1112.
27. **Rief, M., J. Pascual, M. Saraste, and H. E. Gaub.** 1999. Single molecule force spectroscopy of spectrin repeats: low unfolding forces in helix bundles. J. Mol. Biol. **286:**553–561.
28. **Schwaiger, I., C. Sattler, D. R. Hostetter, and M. Rief.** 2002. The myosin coiled-coil is a truly elastic protein structure. Nat. Materials **1:**232–235.